

Rotenone inhibits mammalian cell proliferation by inhibiting microtubule assembly through tubulin binding

Pallavi Srivastava and Dulal Panda

School of Biosciences and Bioengineering, Indian Institute of Technology, Mumbai, India

Keywords

centrosome; microtubule assembly dynamics; microtubules; mitosis; rotenone

Correspondence

D. Panda, School of Biosciences and Bioengineering, Indian Institute of Technology Bombay, Powai, Mumbai 400076, India
Fax: +91 222 572 3480
Tel: +91 222 576 7838
E-mail: panda@iitb.ac.in

(Received 17 April 2007, revised 7 July 2007, accepted 18 July 2007)

doi:10.1111/j.1742-4658.2007.06004.x

Rotenone, a widely used insecticide, has been shown to inhibit mammalian cell proliferation and to depolymerize cellular microtubules. In the present study, the effects of rotenone on the assembly of microtubules in relation to its ability to inhibit cell proliferation and mitosis were analyzed. We found that rotenone inhibited the proliferation of HeLa and MCF-7 cells with half maximal inhibitory concentrations of $0.2 \pm 0.1 \mu\text{M}$ and $0.4 \pm 0.1 \mu\text{M}$, respectively. At its effective inhibitory concentration range, rotenone depolymerized spindle microtubules of both cell types. However, it had a much stronger effect on the interphase microtubules of MCF-7 cells compared to that of the HeLa cells. Rotenone suppressed the reassembly of microtubules in living HeLa cells, suggesting that it can suppress microtubule growth rates. Furthermore, it reduced the intercentrosomal distance in HeLa cells at its lower effective concentration range and induced multipolar-spindle formation at a relatively higher concentration range. It also increased the level of checkpoint protein BubR1 at the kinetochore region. Rotenone inhibited both the assembly and the GTP hydrolysis rate of microtubules *in vitro*. It also inhibited the binding of colchicine to tubulin, perturbed the secondary structure of tubulin, and reduced the intrinsic tryptophan fluorescence of tubulin and the extrinsic fluorescence of tubulin-1-anilinonaphthalene-8-sulfonic acid complex, suggesting that it binds to tubulin. A dissociation constant of $3 \pm 0.6 \mu\text{M}$ was estimated for tubulin-rotenone complex. The data presented suggest that rotenone blocks mitosis and inhibits cell proliferation by perturbing microtubule assembly dynamics.

Rotenone, an agricultural pesticide, is known to inhibit microtubule polymerization and to arrest cell cycle progression at mitosis [1–3]. Recently obtained evidence indicates that systematic administration of rotenone in experimental rats induces degeneration of dopaminergic neurons and produces symptoms that are similar to those observed in Parkinson's disease [4–6]. Although the involvement of rotenone in Parkinson's disease is still under debate [7], it has been suggested that microtubule depolymerization by rotenone may cause the degeneration of dopaminergic neurons

in the substantia nigra, which is believed to be one of the main causes of Parkinson's disease [6–9]. Rotenone is also suggested to induce neurodegeneration by accumulating misfolded tubulin [10]. Furthermore, it has been indicated that rotenone causes aggregation of γ -tubulin in mesencephalic cells [11]. Neurotrophic factors, such as nerve growth factor, brain derived neurotrophic factor and glial cell-line derived neurotrophic factor, have been demonstrated to attenuate the effect of rotenone on midbrain neurons [6]. The microtubule stabilizing agent paclitaxel provides protective effects

Abbreviations

ANS, 1-anilinonaphthalene-8-sulfonic acid; DAPI, 4',6-diamidino-2-phenylindole; IC₅₀, half-maximal inhibitory concentration; MAP, microtubule-associated protein; PI, propidium iodide.

against rotenone-induced toxicity whereas microtubule depolymerizing agents, such as colchicine and nocodazole, produce a effect similar to that of rotenone on dopaminergic neurons [6]. Rotenone has been shown to depolymerize cellular microtubules [1,2] and to inhibit the binding of colchicine to tubulin [2].

Rotenone is also known to inhibit complex I of the oxidative phosphorylation chain of the mitochondrial respiration [12,13]. It has been hypothesized that the inhibition of complex I formation leads to ATP depletion, which in turn induces oxidative stress in cells [14]. Rotenone is also known to induce apoptosis in a variety of cell types and several mechanisms, such as activation of the Jun N-terminal kinase pathway, involvement of the caspase activated DNAase, the redistribution of p53 and the activation of Bad, have been suggested as possible mechanisms for rotenone-induced apoptosis [15–20]. However, the mechanism by which it inhibits cell proliferation at mitosis is not clear.

In the present study, we analyzed the antiproliferative mechanism of action of rotenone in relation to its ability to affect cellular microtubules using HeLa and MCF-7 cells. Our results provide significant insight with respect to the antiproliferative mechanism of action of rotenone.

Results

Effects of rotenone on the proliferation HeLa and MCF-7 cells

Rotenone inhibited the proliferation of HeLa and MCF-7 cells in a concentration dependent manner (Fig. 1A). The half-maximal inhibitory concentration (IC_{50}) of rotenone for HeLa and MCF-7 was determined to be $0.2 \pm 0.1 \mu\text{M}$, and $0.4 \pm 0.1 \mu\text{M}$, respectively.

The effects of rotenone on the cell cycle progression of HeLa and MCF-7 cells were determined. The mitotic index was found to increase in both cell types compared to vehicle-treated cells (Fig. 1B). However, the mitotic arrest was found to be stronger in HeLa cells than in MCF-7 cells (Fig. 1B). After 24 h of incubation with $0.2 \mu\text{M}$ and $0.5 \mu\text{M}$ rotenone, $34 \pm 4\%$; and $68 \pm 6\%$ of HeLa cells were found to be blocked at mitosis, respectively. The concentration of rotenone required to arrest 50% of the HeLa cells at mitosis (MB_{50}) was estimated to be $0.35 \pm 0.12 \mu\text{M}$, which was comparable to the IC_{50} ($0.2 \pm 0.1 \mu\text{M}$). However, $32 \pm 5\%$ of the MCF-7 cells were found to be arrested at mitosis in the presence of $1 \mu\text{M}$ ($2.5 \times IC_{50}$) rotenone.

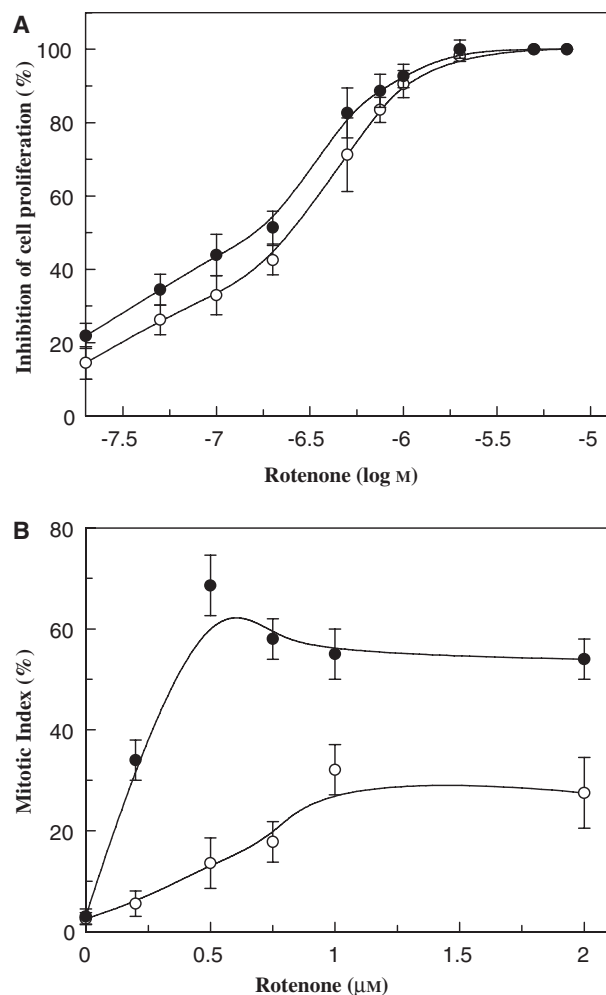


Fig. 1. Effect of rotenone on the proliferation of mammalian cells. (A) Rotenone inhibited the proliferation of HeLa (○) and MCF-7 (●) cells. Cell proliferation was determined after one cell cycle using the sulforhodamine B assay. Error bars indicate SD. (B) Rotenone arrested the cell cycle progression at mitosis of HeLa (●) and MCF-7 (○) cells. At each rotenone concentration, a minimum of 500 cells were counted per experiment. The experiment was repeated five times. Error bars indicate SD.

Rotenone induced apoptotic cell death in HeLa cells

Apoptosis is known to induce several morphological and biochemical changes in the cell. One of these changes is the exposure of phosphatidylserine on the surface of the cell membrane during the early stage of apoptosis. Annexin V is known to bind specifically to phosphatidylserine; therefore, fluorescein isothiocyanate (FITC)-conjugated annexin V was used to detect early apoptosis [21]. Propidium iodide (PI) stains DNA after the disruption of plasma membrane at the late stage of

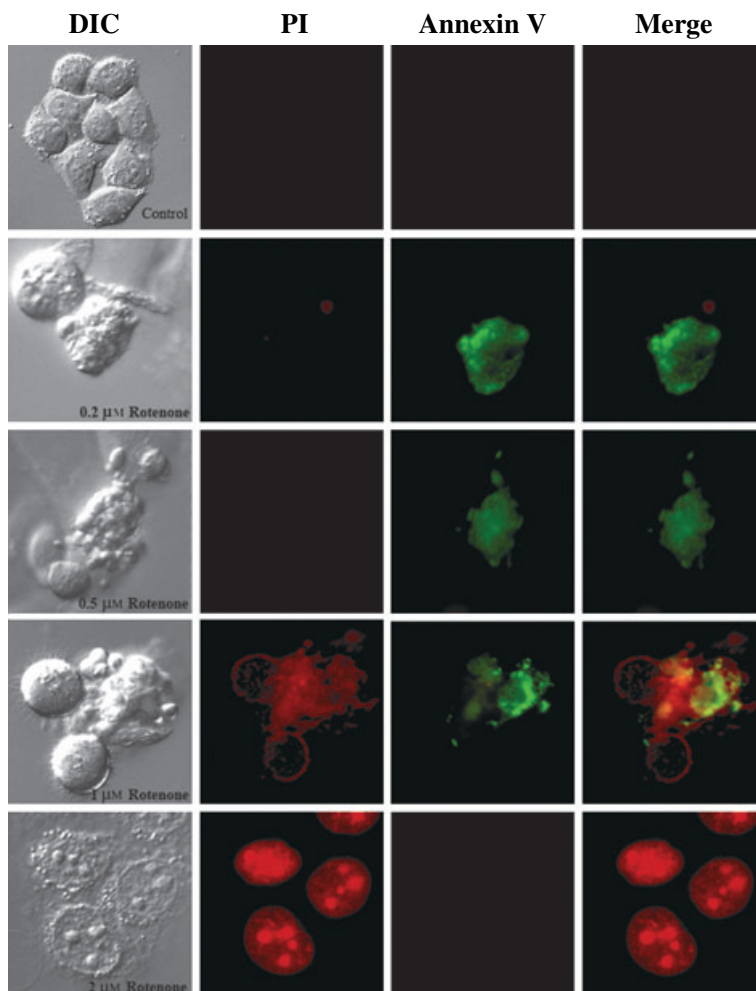


Fig. 2. Rotenone induced apoptosis in mammalian cells. HeLa cells were incubated without or with different concentrations of rotenone for 12 h and stained with annexin V and PI. Panel 1 shows cell morphology using differential interference contrast microscopy. Panel 2 shows PI staining, panel 3 shows annexin V and panel 4 is a merged image of panels 2 and 3. Cells stained with annexin V (green) indicated early apoptotic cells and PI-stained cells (red) indicated late apoptotic/necrotic cells.

apoptosis [22]. Staining the cells with both annexin V and PI helped to differentiate between the early and late apoptotic cells (Fig. 2). At lower concentrations of rotenone, a significant fraction of the HeLa cells were found to be annexin V positive and PI negative. For example, approximately 16% and 23% of all cells were found to be stained with annexin V in the presence of 0.2 μ M and 0.5 μ M rotenone, respectively. At 1 μ M rotenone, approximately 7% of the cells were stained only with annexin V, approximately 14% of the cells were stained with PI only and approximately 23% of the cells were stained with both annexin V and PI. At 2 μ M, approximately 3% of the cells were stained with only annexin V, approximately 46% of the cells were stained with only PI, and approximately 8% of the cells were stained with both annexin V and PI. Differential interference contrast images of the rotenone-treated cells showed typical apoptotic phenotype associated with cell swelling and blebbing.

Rotenone exerted differential effects on the interphase microtubules of HeLa and MCF-7 cells

At a lower effective concentration range (0.2 μ M and 0.5 μ M), rotenone significantly depolymerized the interphase microtubules of MCF-7 cells whereas, at higher concentrations (1 μ M and 2 μ M) of rotenone, the interphase microtubule network of the MCF-7 cells was strongly depolymerized (Fig. 3A). In HeLa cells, the interphase microtubules remained mostly unaffected in the presence 0.2 μ M and 0.5 μ M rotenone. However, high concentration of rotenone (1 μ M or above) caused a significant depolymerization of the interphase microtubules of HeLa cells (Fig. 3A).

Rotenone perturbed mitotic spindle organization

In vehicle-treated cells, normal bipolar spindles were observed with chromosomes arranged in the form of

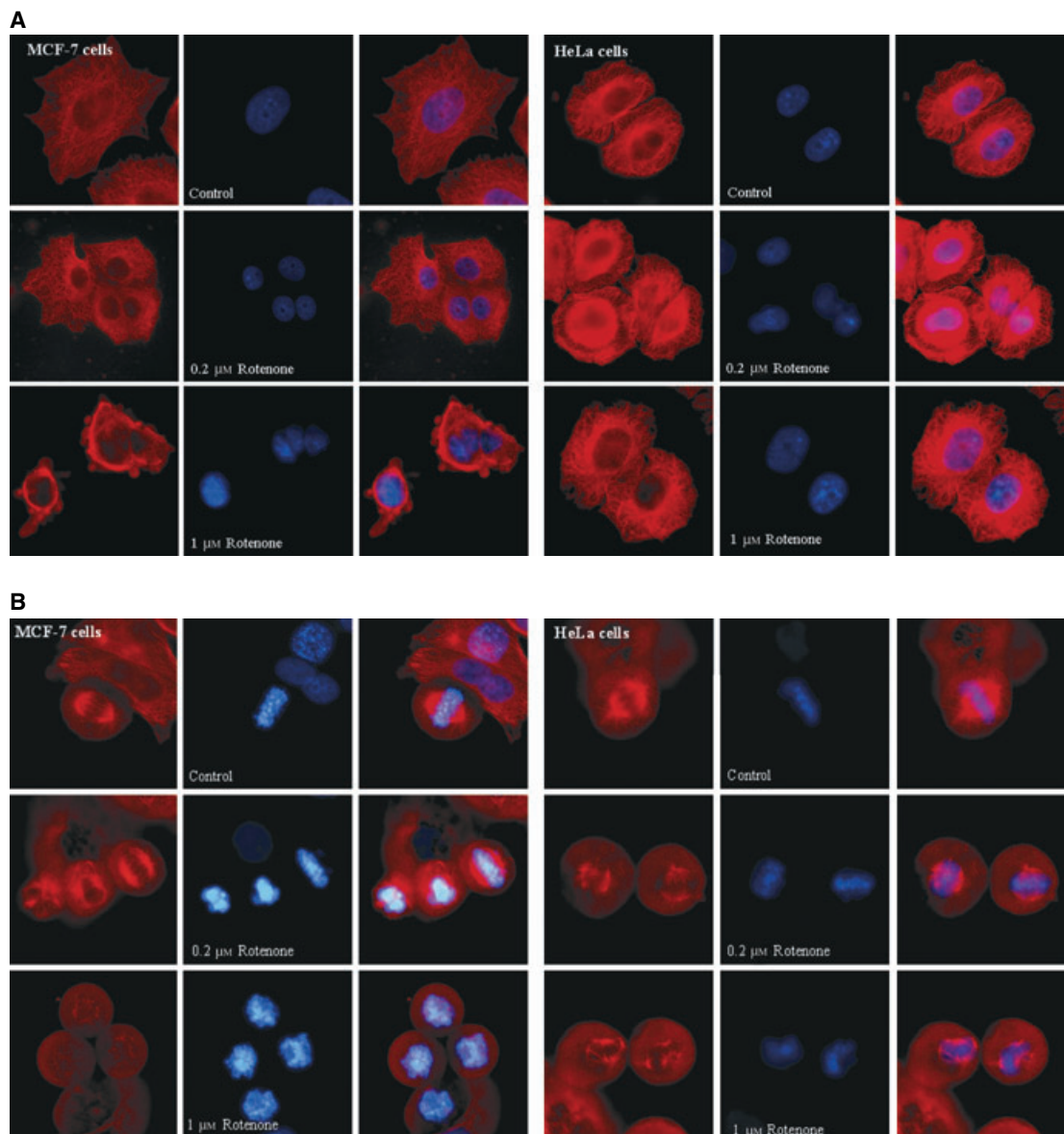


Fig. 3. Effects of rotenone on the microtubules of MCF-7 and HeLa cells. Cells were incubated without or with 0.2 μ M and 1 μ M of rotenone for one cell cycle. Effects of rotenone on the interphase microtubules (A) and mitotic microtubules (B) are shown. Microtubules (red) and chromosomes (blue) were visualized as described in the Experimental procedures.

compact metaphase plates. Effects of rotenone on the spindle microtubules of HeLa and MCF-7 cells were found to be similar (Fig. 3B). Rotenone depolymerized spindle microtubules in a concentration dependent manner. At the lower effective concentration range (0.2 μ M and 0.5 μ M), rotenone perturbed chromosome alignment at the metaphase plate, a few chromosomes were found above or below the metaphase plate and some of the chromosomes were not properly attached with the microtubules. At high concentrations of rotenone, a large number of cells were found to contain

multipolar spindles. For example, approximately 64% and 84% of the HeLa cells contained multipolar spindles in the presence of 1 μ M and 2 μ M rotenone, respectively.

Rotenone suppressed reassembly of microtubules in HeLa cells

Microtubules were depolymerized by incubating the HeLa cells on ice for 1 h. Then, the kinetics of the reassembly of the microtubules in live HeLa cells was

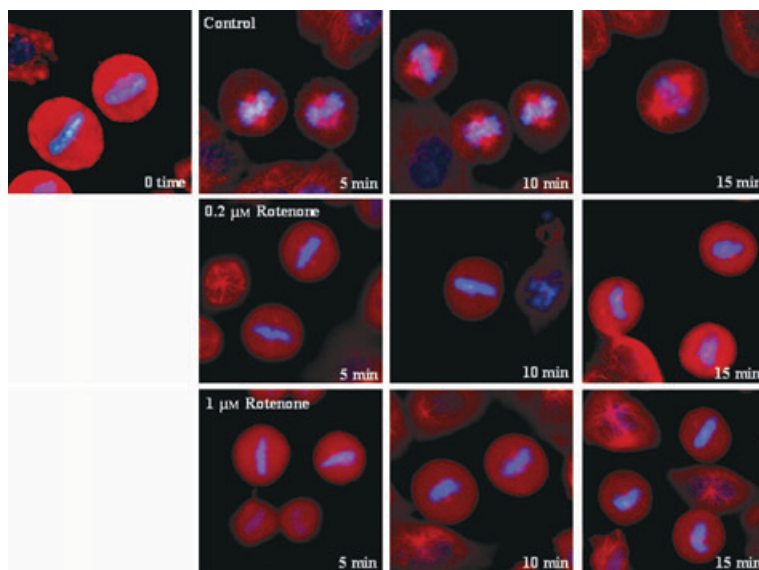


Fig. 4. Rotenone suppressed the reassembly of spindle microtubules in HeLa cells. Cells were fixed at different time intervals. Microtubules (red) and DNA (blue) were stained as described in the Experimental procedures.

monitored by incubating the cells with warm media containing different concentrations of rotenone at 37 °C. In the absence of rotenone, spindle microtubules assembled fast and formed normal spindles (Fig. 4). In the presence of rotenone (0.2 μM and 1 μM), microtubule reassembly was slow and spindles were not observed, even after 15 min of incubation (Fig. 4).

In control cells, depolymerized interphase microtubules reassembled to form normal microtubule network within 10 min of incubation at 37 °C. In the presence of 0.2 μM rotenone, the interphase microtubules did not reassemble till 10 min but well defined microtubule network was observed after 15 min of reassembly. In the presence of 1 μM rotenone, microtubules failed to reassemble even after 15 min of incubation at 37 °C (data not shown).

Rotenone treatment decreased intercentrosomal distance in HeLa cells

Consistent with a previous study [23], the distance between the two centrosomes of a mitotic spindle in HeLa cells was determined to be $11.3 \pm 2 \mu\text{m}$ (Fig. 5). Rotenone reduced the distance between the two spindle poles. For example, the distance between the two centrosomes of a spindle was found to be $5.8 \pm 1.2 \mu\text{m}$ and $4.2 \pm 0.8 \mu\text{m}$ in the presence of 0.2 μM and 0.5 μM rotenone, respectively (Fig. 5). In the presence of 1 μM and 2 μM of rotenone, approximately 64% and 84% of cells contained multipolar spindles and multiple centrosomes. The results suggest that rotenone decreased the spindle length at lower

effective inhibitory concentrations and induced multipolar spindle formation at higher effective inhibitory concentrations (Fig. 5).

Activation of spindle check point protein BubR1 by rotenone

BubR1, a central checkpoint protein, is located at the kinetochores in prometaphase cells [24]. Subsequent to the alignment of chromosomes at the metaphase plate, BubR1 dissociates from the kinetochore region and the cells progress towards anaphase [25]. In the control cells, BubR1 was not detected near the metaphase plate in the mitotic HeLa cells. In the presence of 0.2 μM and 1 μM rotenone, chromosomes were not properly aligned at the metaphase plate and BubR1 was found to be localized with the chromosomes (Fig. 6). The presence of BubR1 protein in the mitotic cells indicated that all kinetochores were not properly attached to microtubules and the required tension was not created between the sister chromatids.

Rotenone inhibited microtubule assembly

Rotenone inhibited the assembly of microtubule-associated protein (MAP)-rich tubulin in a concentration dependent manner (Fig. 7A). The IC_{50} was estimated to be $12 \pm 4.5 \mu\text{M}$. In the absence of rotenone, microtubules formed a dense network of long filaments. Rotenone decreased the mean length of microtubules and also reduced the number of microtubules per grid squares in a concentration dependent manner (Fig. 7B).

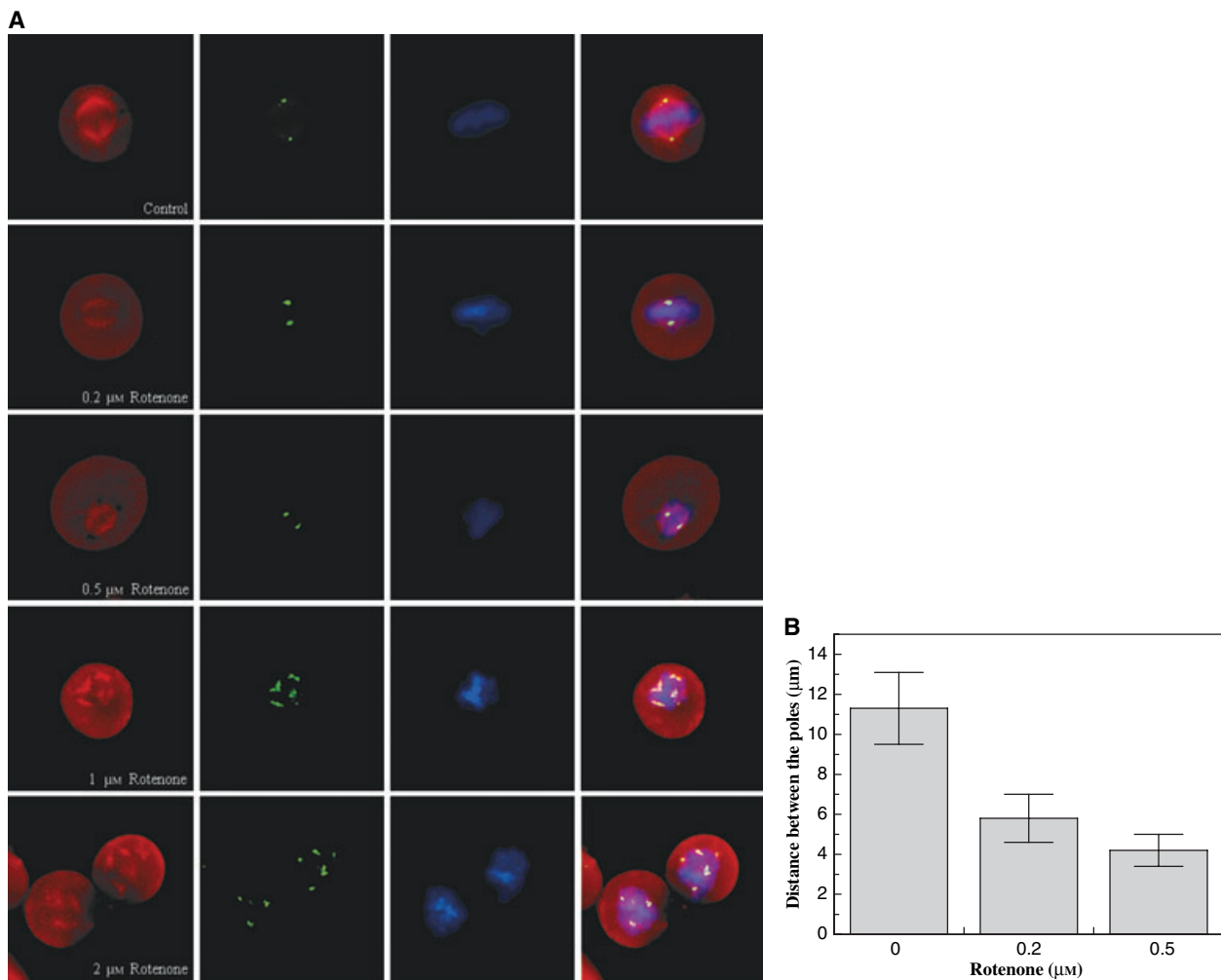


Fig. 5. Rotenone reduced the distance between centrosomes in HeLa cells. (A) Cells were incubated without or with different concentrations (0.2, 0.5, 1 or 2 μ M) of rotenone for 24 h. Centrosomes (green), microtubules (red) and chromosome (blue) are shown. (B) The distance between the centrosome pairs was determined using Image-Pro Plus software. Error bars indicate SD.

Rotenone also inhibited the polymerization of phosphocellulose-purified tubulin in a concentration dependent manner and the IC_{50} of glutamate-induced tubulin assembly occurred in the presence of $20 \pm 3.4 \mu$ M rotenone (data not shown). Furthermore, rotenone strongly suppressed the GTP hydrolysis rate of tubulin assembly (Fig. 8).

Binding of rotenone to tubulin

Rotenone reduced the intrinsic tryptophan fluorescence of tubulin in a concentration dependent manner, suggesting that it induced conformational change in tubulin (Fig. 9A). The dissociation constant (K_d) of the interaction between rotenone and tubulin was calculated to be $3.0 \pm 0.6 \mu$ M (Fig. 9B). Rotenone altered

the far-UV circular dichroism (CD) spectrum of tubulin, indicating that it perturbed the secondary structure of tubulin (data not shown). For example, the CD signal (220 nm) of tubulin in the presence of 50 μ M rotenone was decreased by $13.6 \pm 1.6\%$ ($P < 0.01$) compared to that of the control.

The fluorescence intensity of colchicine increases by several fold after binding to tubulin [26]. Consistent with a previous report [2], we found that preincubation of rotenone with tubulin strongly decreased the fluorescence intensity of tubulin-colchicine complex, indicating that rotenone competes with colchicine for its binding to tubulin (Fig. 10A).

1-Anilinonaphthalene-8-sulfonic acid (ANS), a hydrophobic fluorescence probe, has been found to bind to tubulin at a single site, which is distinct from

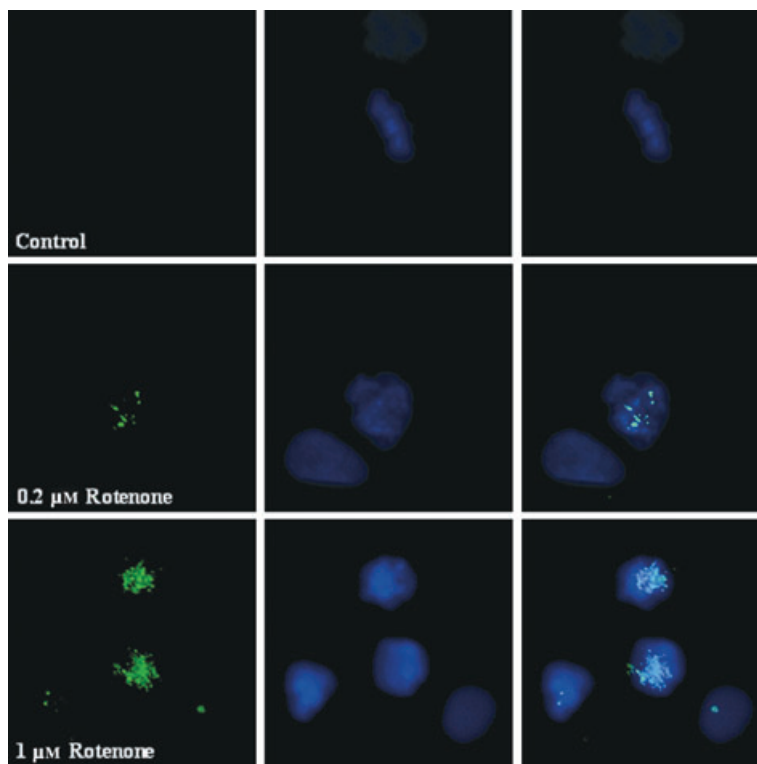


Fig. 6. Rotenone activated the spindle checkpoint protein BubR1. BubR1 (green) and chromosomes (blue) were visualized after staining the cells with mouse anti-BubR1 IgG and DAPI as described in the Experimental procedures.

the colchicine binding site on tubulin [27]. ANS has been used to monitor ligand induced conformational changes in tubulin [28–30]. Rotenone reduced the fluorescence intensity of tubulin–ANS complex in a concentration dependent manner, suggesting that it binds to tubulin (Fig. 10B). The finding also indicated that rotenone either induced conformational changes in tubulin or inhibited the binding of ANS to tubulin. A similar decrease in tubulin–ANS fluorescence was observed with an increasing concentration of rotenone when the experiment was carried out in the presence of 400 μ M ANS instead of 50 μ M ANS (data not shown). For example, rotenone (50 μ M) reduced the fluorescence intensity of tubulin–ANS complex by $25 \pm 4\%$ and $29 \pm 5\%$ compared to that of control when the experiment was performed in the presence of 50 μ M or 400 μ M ANS, respectively, indicating that rotenone does not bind to the ANS binding site on tubulin.

Discussion

In the present study, we found that rotenone perturbed the microtubule organizations and functions in tumor cell lines, activated mitotic check points, inhibited cell proliferation at mitosis and induced programmed cell death in the arrested cells. The apparent effects of rotenone on microtubules correlate well with its antiprolif-

erative and cell killing activity. Furthermore, rotenone was found to bind to tubulin at the colchicine-site with a modest affinity and the binding of rotenone to tubulin perturbed the structure of tubulin. The results suggest that rotenone inhibits microtubule assembly by inducing conformational change in tubulin.

Inhibition of proliferation and mitosis

Rotenone arrested the proliferation of HeLa and MCF-7 cells at mitosis but the mitotic arrest was found to be stronger in HeLa cells compared to that of MCF-7 cells. At its lower effective concentration (approximately IC₅₀), rotenone did not significantly depolymerize the interphase microtubule network in HeLa cells whereas it significantly depolymerized the interphase microtubules of MCF-7 cells. The interphase microtubules of HeLa cells were depolymerized in the presence of relatively high concentrations (1 μ M or above) of rotenone whereas, under similar conditions, the interphase microtubules of MCF-7 cells were strongly depolymerized, suggesting that the interphase microtubules in MCF-7 cells are more susceptible to rotenone than that of the HeLa cells. In interphase cells, microtubules play important roles in transport and trafficking. Due to the depolymerization of the interphase microtubules in MCF-7 cells, the cells might not progress into

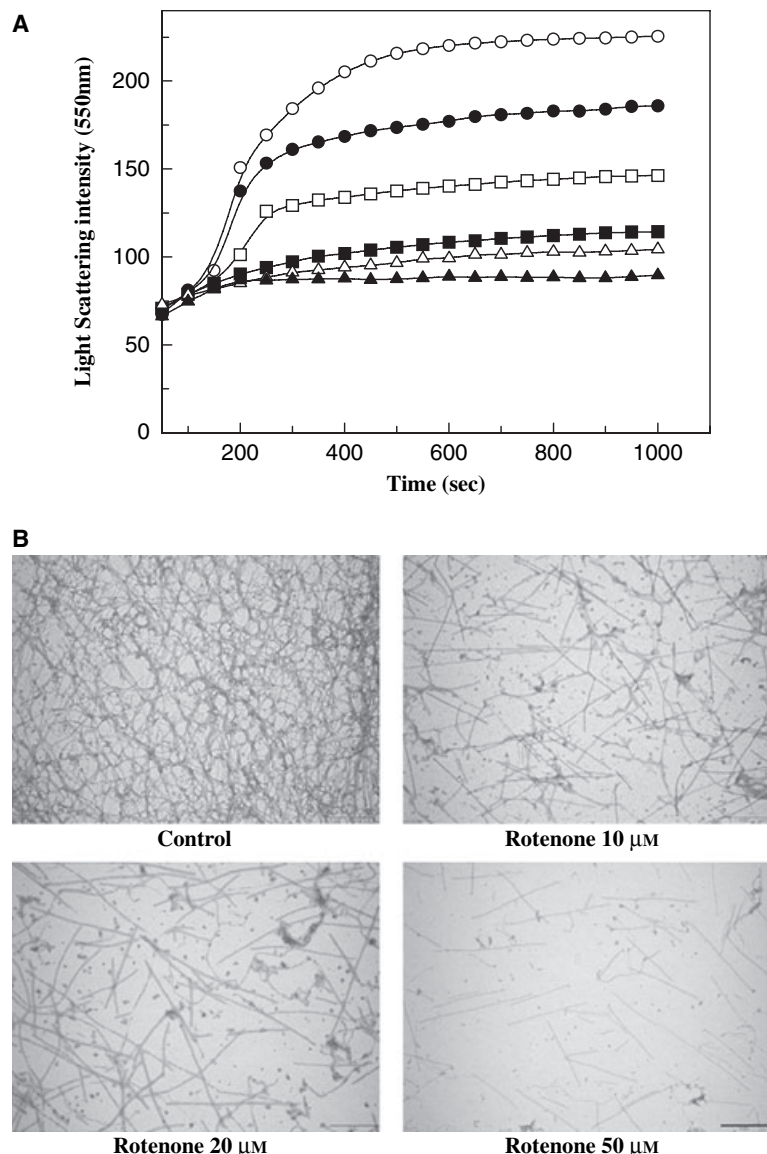


Fig. 7. Rotenone inhibited microtubule assembly *in vitro*. (A) MAP-rich tubulin ($1.2 \text{ mg} \cdot \text{mL}^{-1}$) was polymerized in the absence (○) and presence of 2 μM (●), 5 μM (□), 10 μM (■), 20 μM (△) and 50 μM (▲) rotenone. The kinetics of the assembly reaction was monitored by measuring the light scattering intensity at 550 nm (B). Microtubules were visualized using electron microscope. Images were taken at $\times 11500$ magnification.

mitosis. The effect of rotenone on the spindle microtubules was almost similar in both cell types. At the IC_{50} of rotenone, spindle microtubules were bipolar but spindle length was greatly reduced in both HeLa and MCF-7 cells. At high concentrations of rotenone, multiple spindles were formed in both the cells.

The fidelity of chromosome segregation is thought to be dependent on the proper attachment of kinetochores to microtubules [31–33] and several other factors, such as Mad2, Mad3/BubR1, Bub1, Bub2 and Bub3, and Cdc20, are also believed to play important roles in the cell cycle progression and mitotic arrest [24,34]. In rotenone-treated cells, chromosomes are not properly aligned at the metaphase plate, and aberrant/multipolar spindles were formed. BubR1 was found to be

colocalized along with the chromosomes. BubR1 is an important checkpoint protein, which accumulates at the unattached kinetochore [35]. The accumulation of BubR1 in the rotenone-treated cells indicated that rotenone inhibited the attachment of microtubules to kinetochores.

Effect of rotenone on centrosomes

A low concentration of rotenone caused a decrease in the distance between the two centrosomes in HeLa cells (Fig. 5). The reduction in the distance between the two centrosomes may be due to the depolymerization of microtubules but the role of several factors in centrosome separation, such as actin [36], dynein–dynactin–

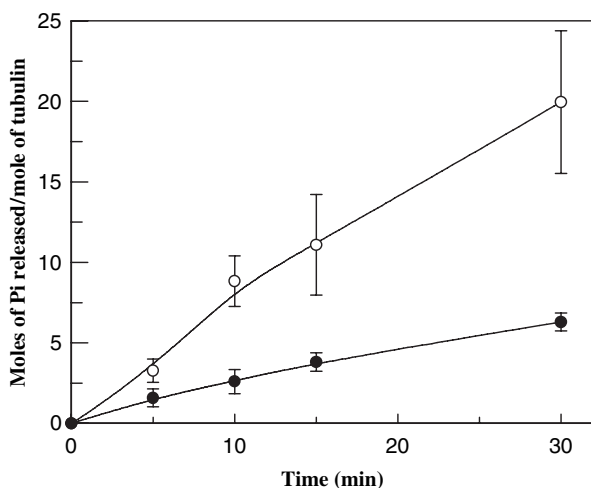


Fig. 8. Effect of rotenone on the GTP hydrolysis rate of tubulin assembly. Tubulin (10 μ M) was polymerized in the absence (○) and presence of 20 μ M rotenone (●). The rate of GTP hydrolysis was measured using the malachite green sodium molybdate assay. Error bars indicate SD.

NuMA [37], Kar3 [38,39], and Eg5 [40], cannot be ignored. Depletion of TACC2, a member of the transforming acidic coiled-coil, leads to reduction in centrosomal distance [41]. Rotenone may also affect these microtubule associated proteins, which lead to the reduction in the intercentrosomal distance. At higher concentrations of rotenone, cells displayed multipolar spindles with more than two centrosomes. Multiple centrosomes can arise either because of the fragmentation or duplication of the centrosomes. Structural protein NuMA, microtubule binding protein Msps/XMAP215 and nuclear core complex protein Mrnp41 (Rae-1) have been reported to play key role in maintaining bipolarity of spindle [42–44]. In addition, rotenone has been suggested to induce aggregation of γ -tubulin in mesencephalic cells [11]. Rotenone may affect the expression of one or more of these proteins, which may result in the formation of the multipolar spindles in cells. Centrosome is an essential part of the spindle and several factors, including microtubule associated proteins, microtubule motors, cross-linking proteins, and actin, are thought to be responsible for its proper function. Taking this into account, it is difficult to suggest a particular reason for the observed centrosomal abnormality in the presence of rotenone. In the presence of low concentrations of rotenone, centrosome aberration was associated with the cell cycle arrest at mitosis. In spite of the defective centrosomes, some of the rotenone-treated cells progressed in the cell cycle, which resulted in chromosomal instability and aneuploidy.

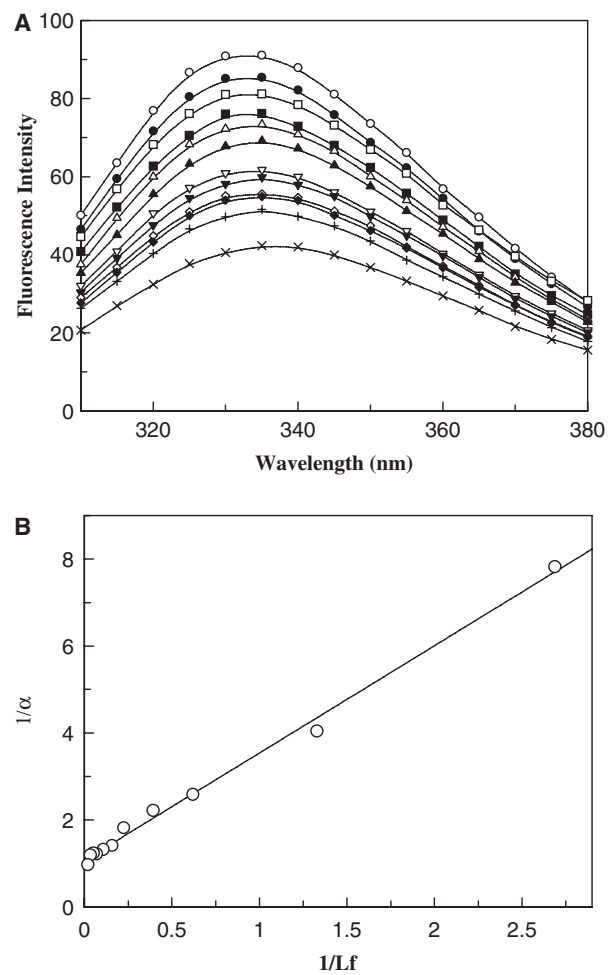


Fig. 9. Effects of rotenone on the intrinsic tryptophan fluorescence of tubulin: Tubulin (1 μ M) was incubated without (○), or with 0.5 μ M (●), 1 μ M (□), 2 (■), 3 μ M (Δ), 5 μ M (\blacktriangle), 7 μ M (∇), 10 μ M (\blacktriangledown), 15 μ M (\diamond), 20 μ M (\blacklozenge), 30 μ M (+) and 50 μ M (x) of rotenone for 30 min at 25 °C. (A) Rotenone reduced the intrinsic fluorescence of tubulin. Emission spectra were recorded using 295 nm as an excitation wavelength. (B) A double reciprocal plot of the binding of rotenone to tubulin is shown. The experiment was performed five times.

Mechanism of action of rotenone

Rotenone reduced the intrinsic tryptophan fluorescence of tubulin and the fluorescence of tubulin-ANS complex, suggesting that rotenone induced conformational changes in tubulin. Rotenone also perturbed the far-UV spectra of tubulin, indicating it altered the secondary structure of tubulin. Together, the results suggest that rotenone inhibited tubulin assembly into microtubules by inducing conformational changes in tubulin. The results show that the effects of rotenone on mammalian cells are similar to the action of benomyl, colchicine and vinblastine [23,30,45].

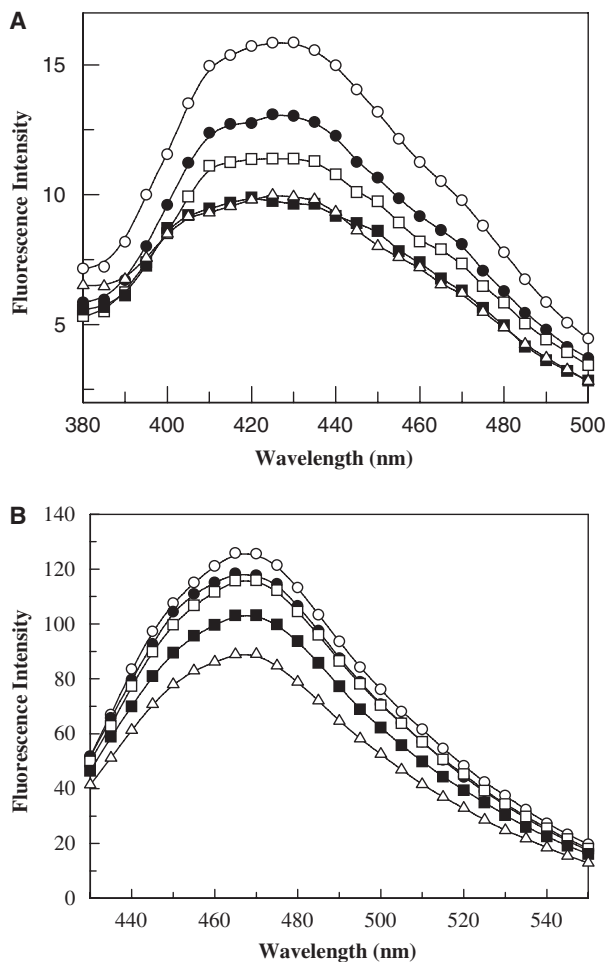


Fig. 10. Effects of rotenone on the ligand binding to tubulin. (A) Rotenone inhibited the binding of colchicine to tubulin. Tubulin (7 μ M) was incubated without (○) or with 5 μ M (●), 10 μ M (□), 20 μ M (■) and 50 μ M (△) rotenone for 30 min. Colchicine (10 μ M) was then added to all of the reaction mixtures and incubated for an additional 60 min at 37 °C. The fluorescence spectra were recorded using 360 nm as an excitation wavelength. The experiment was repeated four times. (B) Rotenone decreased the fluorescence intensity of tubulin-ANS complex. Tubulin (1 μ M) was incubated with 50 μ M ANS for 30 min at 25 °C. Then, the reaction mixtures were incubated in the absence (○) or presence of 5 μ M (●), 10 μ M (□), 25 μ M (■) and 50 μ M (△) rotenone for 30 min. The experiment was performed four times.

Previously, it was suggested that rotenone may cause ATP depletion in cells by inhibiting the complex I of the oxidative phosphorylation chain of mitochondrial respiration and, thus, possibly induce oxidative stress in cells [12,13]. The data presented in the present study, together with those from previous studies [1,2], suggest that rotenone induces mitotic arrest and inhibits the proliferation of cancer cells by perturbing microtubule assembly dynamics.

Experimental procedures

Chemicals and antibodies

Rotenone, GTP, Pipes, sulforhodamine B, colchicine, 4',6-diamidino-2-phenyl-indole (DAPI), mouse monoclonal antibody against α -tubulin, affinity isolated rabbit anti- γ -tubulin IgG, and FITC-conjugated anti-rabbit IgG were purchased from Sigma (St Louis, MO, USA). Phosphocellulose was purchased from Whatman (Maidstone, UK). Antimouse IgG-Alexa 568 conjugate was purchased from Molecular Probes (Eugene, OR, USA). Mouse anti-BubR1 serum was purchased from BD Pharmingen (San Diego, CA, USA). All other reagents were of analytical grade.

Inhibition of cell proliferation

HeLa and MCF-7 cells were cultured in minimal essential medium (Himedia) supplemented with 10% (v/v) fetal bovine serum, 1.5 g L⁻¹ of sodium bicarbonate, and 1% antibiotic antimycotic solution containing streptomycin, amphotericin B, and penicillin. Cells were maintained at 37 °C in a humidified atmosphere of 5% carbon dioxide and 95% air. Cells were seeded at a density of 1 \times 10⁵ cells·mL⁻¹ on 96-well tissue culture plates and incubated with different concentrations of rotenone for one cell cycle (24 h for HeLa and 48 h for MCF-7). Dimethyl sulfoxide was used as a vehicle control. Inhibition of cell proliferation by rotenone was determined by measuring the absorbance of bound sulforhodamine B at 560 nm as described previously [46,47].

Mitotic index

HeLa or MCF-7 cells (6 \times 10⁴ cells·mL⁻¹) were grown on poly L-lysine coated cover slips in 24-well tissue culture plates. The cells were incubated with vehicle (dimethyl sulfoxide) or different concentrations (0.2, 0.5, 0.75, 1 and 2 μ M) of rotenone for one cell cycle. All cells were collected on coverslips by sedimentation (1000 g) using a Labofuge 400R cytopsin centrifuge (Heraeus, Germany). Mitotic index (percentage of mitotic cells) was determined by staining the cells with 1 μ g·mL⁻¹ of DAPI [47]. The cells were counted using a Nikon Eclipse TE 2000-U fluorescence microscope (Nikon, Kanagawa, Japan) with a \times 40 objective. A minimum of 500 cells were counted for each concentration of rotenone per experiment.

Immunofluorescence microscopy

Microtubules, chromosomes, and BubR1 were stained as described previously [23]. Briefly, microtubules were stained using mouse monoclonal anti- α -tubulin IgG (1 : 300 dilution) and Alexa 568-labelled anti-mouse IgG (1 : 400

dilution), and chromosomes were stained with DAPI ($1 \mu\text{g}\cdot\text{mL}^{-1}$). For BubR1 staining, cells were permeabilized with 0.4% triton X-100 and incubated with mouse anti-BubR1 IgG (1 : 1000 dilution) for 1.5 h and then incubated with secondary antibody, FITC-labelled anti-mouse IgG (1 : 500 dilution) for 1 h. The images were captured using a Nikon Eclipse TE 2000-U microscope and analyzed using IMAGE-PRO PLUS software (Media Cybernetics, Silver Spring, MD, USA).

Annexin/PI staining

HeLa cells ($6 \times 10^4 \text{ cells}\cdot\text{mL}^{-1}$) were incubated without or with different concentrations (0.2, 0.5, 1 or 2 μM) of rotenone for 12 h and stained with annexin V and PI using annexin V apoptosis detection kit (Santa Cruz Biotechnology, Santa Cruz, CA, USA) according to manufacturer's instructions.

Effect of rotenone on reassembly of microtubules after cold treatment

HeLa cells were synchronized using thymidine block and then, released into the cell cycle. After 9 h, cells were incubated at 2 °C for 1 h. The cold media was then replaced with warm media containing different concentrations of rotenone. The kinetics of reassembly was monitored by incubating the cells at 37 °C as described previously [23]. Briefly, cells were fixed with 3.7% (v/v) formaldehyde at different time intervals and microtubules and chromosomes were stained as described earlier.

Measurement of intercentrosomal distance

Cells were grown on poly L-lysine coated cover slips and treated with vehicle or rotenone (0.2, 0.5, 1 or 2 μM) for 24 h, and then fixed with 3.7% (v/v) formaldehyde. To visualize the centrosomes and spindle microtubules, cells were processed with primary rabbit anti- γ -tubulin (1 : 2000) and mouse monoclonal α -tubulin (1 : 600) IgG for 1.5 h. Secondary IgG used were anti-rabbit-FITC conjugate (1 : 700) and anti-mouse-Alexa 568 conjugate (1 : 600) [23]. DNA was stained with Hoechst ($0.8 \mu\text{g}\cdot\text{mL}^{-1}$). The distance between the centrosomes was measured by using IMAGE-PRO PLUS software [23].

Purification of tubulin

Goat brain microtubule protein was isolated as described previously [30,48]. MAP-free tubulin was purified from the microtubule protein by phosphocellulose chromatography [48]. Protein concentration was determined by the method of Bradford using bovine serum albumin as standard [49].

Inhibition of microtubule assembly by rotenone *in vitro*

MAP-rich goat brain tubulin ($1.2 \text{ mg}\cdot\text{mL}^{-1}$) was mixed with different concentrations of rotenone in 25 mM pipes at pH 6.8, 3 mM MgSO₄, 1 mM EGTA, and 1 mM GTP on ice. Polymerization was initiated by raising the temperature to 37 °C in the water bath. The rate and extent of polymerization reaction were monitored by attenuation at 550 nm [50,51]. The percentage of inhibition of polymerization was calculated by considering the attenuation intensity of control as 100% after 15 min of assembly.

Tubulin (1.0 $\text{mg}\cdot\text{mL}^{-1}$) was also polymerized in 25 mM pipes at pH 6.8, 3 mM MgSO₄, 1 mM EGTA, 1 mM GTP and 1 M sodium glutamate, in the absence and presence of different concentrations of rotenone for 45 min at 37 °C. The polymers were collected by sedimentation at 88 760 g for 45 min at 30 °C using Optima TM MAX-E ultracentrifuge (Beckman Coulter, Fullerton, CA, USA) and TLA-120.2 rotor.

Electron microscopy

MAP-rich tubulin ($1.2 \text{ mg}\cdot\text{mL}^{-1}$) was polymerized in the absence and presence of different concentrations of rotenone in 25 mM pipes at pH 6.8 containing 3 mM MgSO₄, 1 mM EGTA, and 1 mM GTP. The sample for electron microscopy was prepared as described previously [52]. Briefly, microtubules were fixed with warmed 0.5% glutaraldehyde. Then, the microtubule suspension (20 μL) was placed on carbon-coated grids (300 mesh) and negatively stained with 0.7% uranyl acetate solution. The samples were viewed in a Tecnai G² 120 KV transmission electron microscope (FEI, Eindhoven, the Netherlands).

Measurement of GTPase activity

Tubulin (10 μM) was incubated without or with 20 μM rotenone in 25 mM pipes at pH 6.8, 3 mM MgSO₄, 1 mM EGTA and 1 M monosodium glutamate. The polymerization reaction was started by adding 1 mM GTP and placing the reaction mixtures at 37 °C. The reaction was stopped at specific time intervals by addition of 70% perchloric acid. The rate of GTP hydrolysis was determined using the malachite green sodium molybdate assay [52,53]. The background absorbance was subtracted from all readings.

The binding of rotenone to tubulin

Tubulin (1 μM) was incubated without or with different concentrations (0.5–50 μM) of rotenone at 25 °C for 30 min. The fluorescence spectra were collected using a 0.3 cm path length cuvette in a Jasco FP-6500 fluorescence spectrophotometer (Jasco Inc., Easton, MD, USA). The excitation wavelength was 295 nm. The observed fluores-

cence intensities were corrected for the inner filter effect using the formula $F_c = F_{\text{obs}} \times \text{antilog}[(A_{\text{ex}} + A_{\text{em}})/2]$, where F_c is the corrected fluorescence, F_{obs} is the observed fluorescence, A_{ex} is the absorbance at the excitation wavelength and A_{em} is the absorbance at the emission wavelength [54]. Rotenone reduced the intrinsic fluorescence of tubulin in a concentration dependent manner. The dissociation constant (K_d) of the rotenone and tubulin interaction was determined as described previously [30]. The fraction of the binding site (α) occupied by rotenone was calculated using the equation $\alpha = (F_0 - F_c)/\Delta F_{\text{max}}$, where, F_0 , F_c and ΔF_{max} represent the fluorescence intensity of tubulin in the absence of rotenone, the fluorescence intensity of tubulin in the presence of different concentrations of ligand and the maximum change in the fluorescence intensity of tubulin when it is fully bound with the ligand, respectively. ΔF_{max} was estimated from the y -intercept of the graph $1/(F_c - F_0)$ versus $1/[\text{rotenone}]$. Assuming a single binding site of rotenone per tubulin dimer, K_d was determined using the relationship, $1/\alpha = 1 + K_d/L_f$, where L_f represents the free concentration of rotenone. L_f was determined by subtracting the bound ligand concentration from the total ligand concentration. Five independent experiments were performed.

CD spectra

Tubulin (5 μM) was incubated without or with different concentrations (5, 10, 20 and 50 μM) of rotenone for 30 min at 25 °C. The far-UV CD spectra of tubulin were recorded using a 1 mm path length quartz cuvette in a Jasco spectropolarimeter (model J-810) at 25 °C. Spectra were collected with a scan speed of 200 nm·min⁻¹ and each spectrum was the average of three scans.

Effects of rotenone on the binding of colchicine to tubulin

The fluorescence intensity of colchicine is known to increase by several folds after binding to tubulin [26]. The competition between rotenone and colchicine for tubulin binding was examined using the fluorescence of tubulin-colchicine complex. Tubulin (7 μM) was first incubated without or with different concentrations (5, 10, 20 and 50 μM) of rotenone for 30 min at 37 °C. Colchicine (10 μM) was then added to the reaction mixtures and incubated for an additional 60 min at 37 °C and the fluorescence spectra were recorded. The excitation and emission wavelengths were 360 nm and 430 nm, respectively.

Effect of rotenone on tubulin-ANS complex

Tubulin (1 μM) was incubated with 50 or 400 μM of ANS in 25 mM pipes, pH 6.8, 3 mM MgSO₄ and 1 mM EGTA

for 30 min at 25 °C. Then, the reaction mixtures were incubated without or with different concentrations (5, 10, 25, and 50 μM) of rotenone for an additional 30 min. Emission spectra were recorded using 360 nm as an excitation wavelength. The excitation and emission bandwidths were 5 nm and 10 nm, respectively.

Acknowledgements

The work is supported by National Bioscience Award from the Department of Biotechnology, Government of India to D.P. The authors thank Sophisticated Analytical Instrument Facility (SAIF), IIT Bombay for use of the electron microscopy facility and Renu Mohan and K. Rathinasamy for critical reading of the manuscript.

References

- 1 Meisner HM & Sorensen L (1966) Metaphase arrest of Chinese hamster cells with rotenone. *Exp Cell Res* **42**, 291–295.
- 2 Brinkley BR, Barham SS, Barranco SC & Fuller GM (1974) Rotenone inhibition of spindle microtubule assembly in mammalian cells. *Exp Cell Res* **85**, 41–46.
- 3 Marshall LE & Himes RH (1978) Rotenone inhibition of tubulin self assembly. *Biochim Biophys Acta* **543**, 590–594.
- 4 Alam M & Schmidt WJ (2002) Rotenone destroys dopaminergic neurons and induces parkinsonian symptoms in rats. *Behav Brain Res* **136**, 317–324.
- 5 Betarbet R, Sherer TB, MacKenzie G, Garcia-Osuna M, Panov AV & Greenamyre JT (2000) Chronic systemic pesticide exposure reproduces features of Parkinson's disease. *Nat Neurosci* **3**, 1301–1306.
- 6 Jiang Q, Yan Z & Feng J (2006) Neurotrophic factors stabilize microtubules and protect against rotenone toxicity on dopaminergic neurons. *J Biol Chem* **281**, 29391–29400.
- 7 Richter F, Hamann M & Richter A (2007) Chronic rotenone treatment induces behavioral effects but no pathological signs of Parkinsonism in mice. *J Neurosci Res* **85**, 681–691.
- 8 Ren Y, Liu W, Jiang H, Jiang Q & Feng J (2005) Selective vulnerability of dopaminergic neurons to microtubule depolymerization. *J Biol Chem* **280**, 34105–34112.
- 9 Feng J (2006) Microtubule: a common target for parkin and Parkinson's disease toxins. *Neuroscientist* **12**, 469–476.
- 10 Ren Y, Zhao JH & Feng J (2003) Parkin binds to alpha/beta tubulin and increases their ubiquitination and degradation. *J Neurosci* **23**, 3316–3324.
- 11 Diaz-Corrales FJ, Asanuma M, Miyazaki I, Miyoshi K & Ogawa N (2005) Rotenone induces aggregation of

γ -tubulin protein and subsequent disorganization of the centrosome: relevance to formation of inclusion bodies and neurodegeneration. *Neuroscience* **133**, 117–135.

12 Higgins DS & Greenamyre JT (1996) [3 H]dihydrorotenone binding to NADH: ubiquinone reductase (complex I) of the electron transport chain: an autoradiographic study. *J Neurosci* **16**, 3807–3816.

13 Chance B, Williams GR & Hollunger G (1963) Inhibition of electron and energy transfer in mitochondria. I. Effects of amyta, thiopental, rotenone, progesterone, and methylene glycol. *J Biol Chem* **238**, 418–431.

14 Sherer TB, Betarbet R, Testa CM, Seo BB, Richardson JR, Kim JH, Miller GW, Yagi T, Matsuno-Yagi A & Greenamyre JT (2003) Mechanism of toxicity in rotenone models of Parkinson's disease. *J Neurosci* **23**, 10756–10764.

15 Hartley A, Stone JM, Heron C, Cooper JM & Schapira AH (1994) Complex I inhibitors induce dose-dependent apoptosis in PC12 cells: relevance to Parkinson's disease. *J Neurochem* **63**, 1987–1990.

16 Wolvekang EJ, Johnson KL, Krauer K, Ralph SJ & Linnane AW (1994) Mitochondrial respiratory chain inhibitors induce apoptosis. *FEBS Lett* **339**, 40–44.

17 Newhouse K, Hsuan Chang SH, Cai B, Wang Y & Xia Z (2004) Rotenone-induced apoptosis is mediated by p38 and JNK MAP kinases in human dopaminergic SH-SY5Y cells. *Toxicol Sci* **79**, 137–146.

18 Tsuruta T, Oh-hashi K, Ueno Y, Kitade Y, Kiuchi K & Hirata Y (2007) RNAi knockdown of caspase-activated DNase inhibits rotenone-induced DNA fragmentation in HeLa cells. *Neurochem Int* **50**, 601–606.

19 Diaz-Corrales FJ, Asanuma M, Miyazaki I, Miyoshi K & Ogawa N (2006) Centrosome overduplication induced by rotenone treatment affects the cellular distribution of p53 tumor suppressor protein in the neuroblastoma B65 cell line. *Psychiatry Clin Neurosci* **60**, S18–S26.

20 Watabe M & Nakaki T (2004) Rotenone induces apoptosis via activation of Bad in human dopaminergic SH-SY5Y cells. *J Pharmacol Exp Ther* **311**, 948–953.

21 Aubry JP, Blaecke A, Lecoanet-Henchoz S, Heannin P, Herbault N, Caron G, Moine V & Bonnefond JY (1999) Annexin V used for measuring apoptosis in the early events of cellular cytotoxicity. *Cytometry* **37**, 197–204.

22 O'Brien MC & Bolton WE (1995) Comparison of cell viability probes compatible with fixation and permeabilization for combined surface and intracellular staining in flow cytometry. *Cytometry* **19**, 243–255.

23 Rathinasamy K & Panda D (2006) Suppression of microtubule dynamics by benomyl decreases tension across kinetochore pairs and induces apoptosis in cancer cells. *FEBS J* **273**, 4114–4128.

24 Hoffman DB, Pearson CG, Yen TJ, Howell BJ & Salmon ED (2001) Microtubule-dependent changes in assembly of microtubule motor proteins and mitotic spindle checkpoint proteins at PtK1 kinetochores. *Mol Biol Cell* **12**, 1995–2009.

25 Zhou J, Yao J & Joshi HC (2002) Attachment and tension in the spindle assembly checkpoint. *J Cell Sci* **115**, 3547–3555.

26 Bhattacharyya B & Wolff J (1974) Promotion of fluorescence upon binding of colchicine to tubulin. *Proc Natl Acad Sci USA* **71**, 2627–2631.

27 Bhattacharyya B & Wolff J (1975) The interaction of 1-anilino-8-naphthalene sulfonate with tubulin: a site independent of the colchicine-binding site. *Arch Biochem Biophys* **167**, 264–269.

28 Gupta K & Panda D (2002) Perturbation of microtubule polymerization by quercetin through tubulin binding: a novel mechanism of its antiproliferative activity. *Biochemistry* **41**, 13029–13038.

29 Lee JC, Harrison D & Timasheff SN (1975) Interaction of vinblastine with calf brain microtubule protein. *J Biol Chem* **250**, 9276–9282.

30 Gupta K, Bishop J, Peck A, Brown J, Wilson L & Panda D (2004) Antimitotic antifungal compound benomyl inhibits brain microtubule polymerization and dynamics and cancer cell proliferation at mitosis by binding to a novel site in tubulin. *Biochemistry* **43**, 6645–6655.

31 Amon A (1999) The spindle checkpoint. *Curr Opin Genet Dev* **9**, 69–75.

32 Li X & Nicklas RB (1995) Mitotic forces control a cell cycle checkpoint. *Nature* **373**, 630–632.

33 Rieder CL, Cole RW, Khodjakov A & Sluder G (1995) The checkpoint delaying anaphase in response to chromosome monoorientation is mediated by an inhibitory signal produced by unattached kinetochores. *J Cell Biol* **130**, 941–948.

34 Sudakin V, Chan GK & Yen TJ (2001) Checkpoint inhibition of the APC/C in HeLa cells is mediated by a complex of BUBR1, BUB3, CDC20, and MAD2. *J Cell Biol* **154**, 925–936.

35 Cleveland DW, Mao Y & Sullivan KF (2003) Centromeres and kinetochores: from epigenetics to mitotic checkpoint signaling. *Cell* **112**, 407–421.

36 Uzbekov R, Kireyev I & Prigent C (2002) Centrosome separation: respective role of microtubules and actin filaments. *Mol Biol Cell* **94**, 275–288.

37 Merdes A, Heald R, Samejima K, Earnshaw WC & Cleveland DW (2000) Formation of spindle poles by dynein/dynactin dependent transport of NuMA. *J Cell Biol* **149**, 851–862.

38 Tanaka K, Mukae N, Dewar H, van Breugel M, James EK, Prescott AR, Antony C & Tanaka TU (2005) Molecular mechanisms of kinetochore capture by spindle microtubules. *Nature* **434**, 987–994.

39 Meluh PB & Rose MD (1990) KAR3, a kinesin-related gene required for yeast nuclear fusion. *Cell* **60**, 1029–1041.

40 Enos AP & Morris NR (1990) Mutation of a gene that encodes a kinesin-like protein blocks nuclear division in *A. nidulans*. *Cell* **60**, 1019–1027.

41 Doua Z, Dingb X, Zereshkid A, Zhang Y, Zhang J, Wang F, Sunc J, Huang H & Yao X (2004) TTK kinase is essential for the centrosomal localization of TACC2. *FEBS Lett* **572**, 51–56.

42 Gaglio T, Dionne MA & Compton DA (1997) Mitotic spindle poles are organized by structural and motor proteins in addition to centrosomes. *J Cell Biol* **138**, 1055–1066.

43 Cullen CF & Okura H (2001) Msps protein is localized to a centrosomal poles to ensure bipolarity of *Drosophila* meiotic spindles. *Nat Cell Biol* **3**, 637–642.

44 Gergely F, Kidd D, Jeffers K, Wakefield JG & Raff JW (2000) D-TACC: a novel centrosomal protein required for normal spindle function in the early *Drosophila* embryo. *EMBO J* **19**, 241–252.

45 Jordan MA & Wilson L (2004) Microtubules as a target for anticancer drugs. *Nat Rev Cancer* **4**, 253–265.

46 Skehan P, Storeng R, Scudiero D, Monks A, McMahon J, Vistica D, Warren JT, Bokesh H, Kenney S & Boyd MR (1990) New colorimetric cytotoxicity assay for anticancer drug screening. *J Natl Cancer Inst* **82**, 1107–1112.

47 Mohan R, Banerjee M, Ray A, Manna T, Wilson L, Owa T, Bhattacharyya B & Panda D (2006) Antimitotic sulfonamides inhibit microtubule assembly dynamics and cancer cell proliferation. *Biochemistry* **45**, 5440–5449.

48 Hamel E & Lin CM (1981) Glutamate-induced polymerization of tubulin: characteristics of the reaction and application to the large-scale purification of tubulin. *Arch Biochem Biophys* **209**, 29–40.

49 Bradford MM (1976) A rapid and sensitive method for the quantitation of microgram quantities of protein utilizing the principle of protein–dye binding. *Anal Biochem* **72**, 248–254.

50 Gaskin F, Cantor CR & Shelanski M (1974) Turbidimetric studies of the in vitro assembly and disassembly of porcine neurotubules. *J Mol Biol* **89**, 737–755.

51 Mohan R, Rastogi N, Namboothiri IN, Mobin SM & Panda D (2006) Synthesis and evaluation of alpha-hydroxymethylated conjugated nitroalkenes for their anticancer activity: inhibition of cell proliferation by targeting microtubules. *Bioorg Med Chem* **14**, 8073–8085.

52 Gupta KK, Bharne SS, Rathinasamy K, Naik NR & Panda D (2006) Dietary antioxidant curcumin inhibits microtubule assembly through tubulin binding. *FEBS J* **273**, 5320–5332.

53 Lanzetta PA, Alvarez LJ, Reinach PS & Candia OA (1979) An improved assay for nanomole amounts of inorganic phosphate. *Anal Biochem* **100**, 95–97.

54 Lakowicz JR (1999) *Principles of Fluorescence Spectroscopy*, 2nd edn. Kluwer Academic/Plenum Publishers, New York, NY.